Volume 6 | Number 25 | 7 July 2018 | Pages 6607–6886

Journal of Materials Chemistry C

Materials for optical, magnetic and electronic devices

rsc.li/materials-c

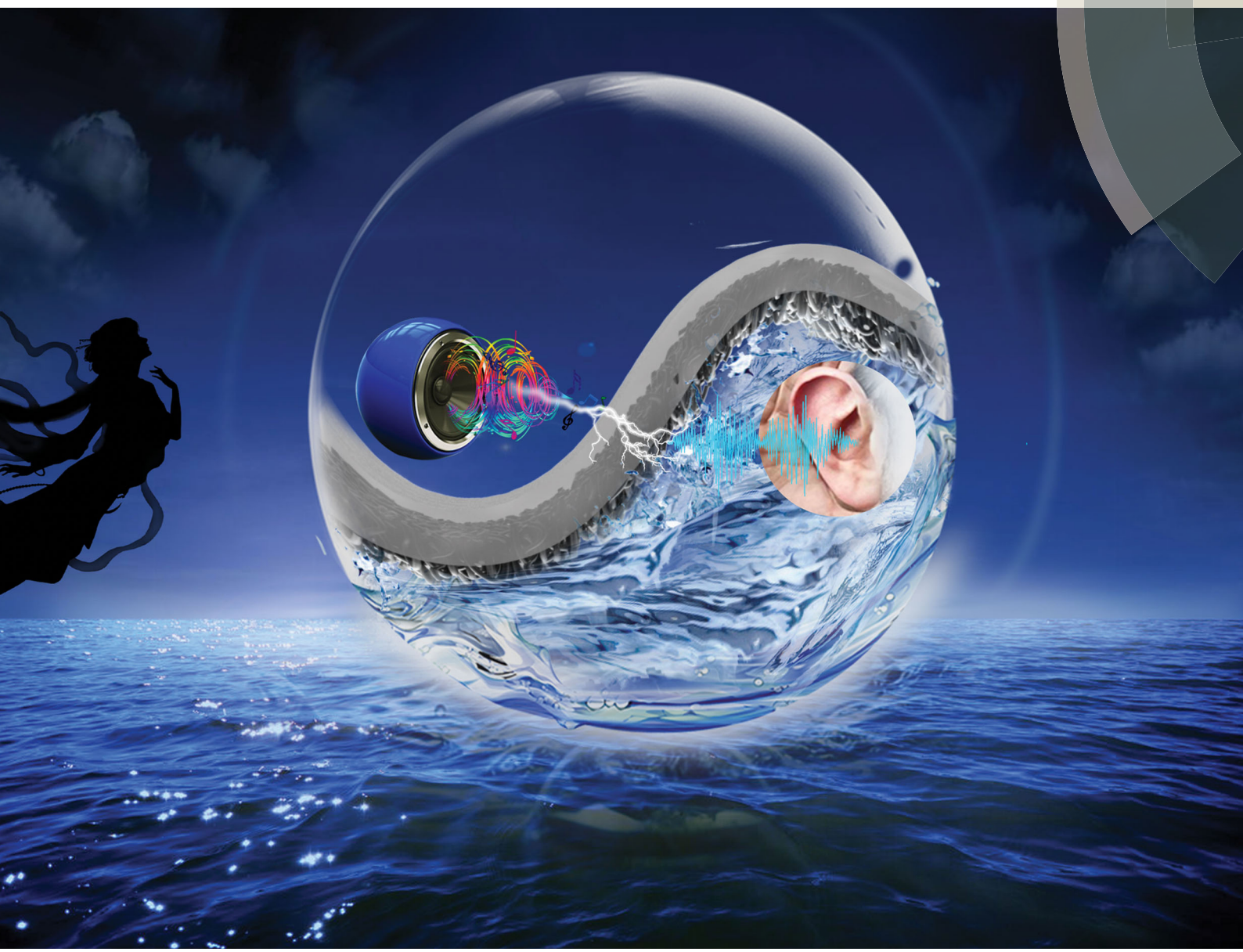

ISSN 2050-7526

ROYAL SOCIETY OF CHEMISTRY

PAPER

Peng Xiao, Youju Huang, Tao Chen *et al.*

Scalable fabrication of free-standing, stretchable CNT/TPE ultrathin composite films for skin adhesive epidermal electronics

Journal of Materials Chemistry C

PAPER

View Article Online
View Journal | View Issue

Cite this: J. Mater. Chem. C, 2018, 6, 6666

Scalable fabrication of free-standing, stretchable CNT/TPE ultrathin composite films for skin adhesive epidermal electronics†

Yun Liang,[ab] Peng Xiao,*[ab] Shuai Wang,[ab] Jiangwei Shi,[a] Jiang He,[ab] Jiawei Zhang,[ab] Youju Huang*[ab] and Tao Chen*[ab]

Received 9th February 2018,
Accepted 4th May 2018

DOI: 10.1039/c8tc00711j

rsc.li/materials-c

Wearable electronics have drawn extensive interest on account of their potential applications in smart human–machine interfaces, wearable human-health monitors and mimicking biological organs. However, the scalable and cost-effective fabrication of self-adhesive and easily transferred flexible ultrathin films is still challenging. Herein, a simple and highly efficient strategy was proposed for an ultrathin, self-standing and self-adhesive macroscopic CNT/TPE hybrid film at the air/water interface. Due to its distinctive ultrathin feature, the obtained film can be directly attached to the skin surface for real-time human physiological behaviour detection. Additionally, the free-standing hybrid film can be employed for the effective detection of tiny airflow changes and even acoustic vibration.

Introduction

Flexible electronics, enabling potential applications in human-health monitoring or mimicking the function of some biological organs, has blossomed over the last few years due to its portable, miniaturized, and wearable characteristics.[1–6] Specifically, ultrathin, self-adhesive and skin-conformal integration of epidermal electronics, targeting good experiences, excellent adaptability, biocompatibility and long-term monitoring, is highly desirable for the next generation of wearable sensing systems.[7–11] Recently, new concepts of nanomaterial composites, fabrication strategies and well-designed devices have been introduced into electronic systems for achieving high performance.[12–15]

One recent example is the utilization of a micro-structured poly(dimethylsiloxane) (PDMS) topographical film (several hundreds of micrometers) to guide conductive graphene patterns for skin-conformal sensors.[16] More recently, strong self-adhesive strain sensors were successfully designed through the introduction of viscous vinylsiloxane onto pillared PDMS patterns.[17] Moreover, aiming at unprecedented experiences at human–machine interfaces, Someya *et al.* creatively developed a non-immunostimulatory, gas-permeable and conformal Au nanomesh electronic device, which is super-thin enough to be imperceptible to humans.[18] Despite tremendous advances being significantly achieved to realize skin conformity, self-adhesion and gas-permeability, this is still challenging due to the limited lateral dimensions, high costs, sophisticated, time-consuming preparation processes, *etc.* Thus, a cost-effective, large-area and transferrable alternative is eagerly desired for epidermal electronic devices.

The air/water interface with a molecular level is considered as an ideal platform for well-controlled self-assembly and two-dimensionally confined asymmetric physical/chemical reactions.[19–22] By introducing specific elements at the air/water interface, large-area and transferrable monolayers could be easily realized without the limitations of rigid substrates.[23,24] Due to the flexibility of interfacial modification, the monolayers at the interface could be further decorated with the desired chemical groups or integrated into functional polymers with adjusted thickness for targeted applications.[25] More recently, our group has developed a simple, highly efficient and cost-effective strategy to fabricate a closely-packed carbon nanotube (CNT) film at the air/water interface through the combination of Marangoni-induced self-assembly and capillary force driving compression.[26] Since the thermoplastic elastomer (TPE) is reversibly elastic, easily prepared and nontoxic,[27,28] it is regarded as a good alternative for a superelastic matrix in flexible electronics application.[28]

Herein, we present a recent advance in which TPE can be asymmetrically introduced into the free-standing CNT film surface at the air/water interface through an interfacial modification strategy.

[a] Key Laboratory of Marine Materials and Related Technologies, Zhejiang Key Laboratory of Marine Materials and Protective Technologies, Ningbo Institute of Materials Technology and Engineering, Chinese Academy of Sciences, Ningbo 315201, China. E-mail: tao.chen@nimte.ac.cn, yjhuang@nimte.ac.cn, xiaopeng@nimte.ac.cn
[b] University of Chinese Academy of Sciences, 19A Yuquan Road, Beijing 100049, China

† Electronic supplementary information (ESI) available. See DOI: 10.1039/c8tc00711j

This approach allows the formation of a large-area, well-defined and low-cost Janus CNT/TPE hybrid film. By tuning the structural parameters, the hybrid film exhibits ultrathin, free-standing and self-adhesive features and asymmetric electrical performance. When employed as a strain sensor, it can act as a self-adhesive epidermal electronic device to monitor body motion behaviours and the physiological pulse with high quality. Additionally, unlike the common application fields of strain sensors, the free-standing Janus film can be employed for remote real-time acoustic recognition, showing potential applications in artificial eardrums.

Experimental section

Materials

The raw CNTs (diameter, about 10–30 nm; length, about 10–30 μm; –COOH %, about 5 wt%) with a purity of over 95% were acquired from Chengdu Organic Chemistry Co., Ltd. The TPE was purchased from Gainshine, China. Other solvents and reagents were obtained from Sinopharm Chemical Reagent Co., Ltd. and used as received. PDMS substrates were fabricated from Sylgard 184 (Dowcorning, US) on Plastic Petri dishes (the ratio between components A and B was 1 : 10).

Preparation of CNT films at the air/water interface

The CNT films were prepared according to previous Langmuir–Blodgett assembly methods with some alterations.[26,29] Typically, different masses of CNTs (20 mg, 40 mg, 60 mg and 100 mg) were first dispersed in 200 mL anhydrous ethanol solution, followed by strong ultrasonication for 2 h using an ultrasonic bath to form a stable dispersion with the appropriate aging time. Subsequently, 35 mL of the resultant uniform CNT dispersion was dropped onto a deionized water surface after stabilization for about 30 min, the capillary substance like tissues or microporous sponges were selected to put on one side of the interface to quickly siphon water from the system, followed by a prominent decrease of the Langmuir area. Notably, the homogeneous Langmuir layers were closely packed toward the opposite direction of the siphoning direction. When the movement of the film stopped and further siphoning could not drive the film, the resulting film was ultimately formed, indicating a closely packed structure.

Preparation of CNT/TPE hybrid films at the air/water interface

The different masses of TPE elastomer (0.4 g and 2 g) were dissolved in 200 mL *N*-heptane by strong ultrasonication for 30 min. Subsequently, 35 mL TPE solution was sprayed onto the as prepared CNT film surface at a speed of 20 mL min^{-1} by a sprayer. The TPE gradually precipitates as the solvent evaporates, and after the solvent was completely evaporated, a uniform CNT/TPE hybrid film was formed.

Sensor preparation

The CNT/TPE hybrid films (thickness, about 2 μm or 18 μm) were coated on PDMS substrates (thickness, about 1 mm) by directly attaching PDMS onto the side of the TPE, and then cutting into strips with a size of 25 mm × 3 mm × 1 mm ($L_0 \times W_0 \times t_0$) for the gauge factor (GF) test. Notably, the other applications directly used the initial CNT/TPE hybrid films without further treatment.

Characterization

Scanning electron microscopy was performed to observe the micromorphology with a Hitachi S-4800 cold field emission SEM at an accelerating voltage of 8 kV. An Instron 5567 universal testing machine was used to stretch the coated CNT/TPE sensor on a piece of PDMS with one end fixed and the other end linearly elongated at constant speed. Resistance measurements were carried out by connecting the two ends of the CNT/TPE hybrid film sensor to an Electrochemical Workstation (CH Instruments, CHI660E, Chenhua Co., Shanghai, China), with conductive copper wires to record the real-time current (I) flowing through the film under a constant voltage (V_0) of 1 V, while the real-time resistance (R) was calculated by the equation $R = V_0/I$. The software Praat was used to analyze the time domain spectrogram of the music.

Results and discussion

The strategy for fabricating an ultrathin and self-adhesive CNT/TPE hybrid ultrathin film at the air/water interface is schematically illustrated in Fig. 1. The method is relatively simple and highly efficient in the absence of expensive instruments and complex preparation procedures. Firstly, The CNT films were prepared using the modified Langmuir–Blodgett method. When the CNT dispersion was sprayed onto the water surface, the CNTs were rapidly pushed outward from the ethanol-rich regions with low surface tension to the water-rich regions with high surface tension owing to the strong Marangoni forces. The homogeneous CNT thin film with a loosely compacted state could be further compressed driven by porous sponge induced capillary forces. Due to the different surface tension, it further induced the motion of the CNTs towards the opposite direction. As a result, a closely packed CNT thin film was finally achieved (Fig. 1a). Secondly, TPE *N*-heptane solution was sprayed onto the as-prepared CNT film surface. Thanks to the Marangoni effects, the TPE/heptane solution with low surface tension spread spontaneously on the water surface with high surface tension. With the evaporation of the heptane, the TPE film gradually formed. Finally, a uniform CNT/TPE hybrid Janus film was formed at the air/water interface (Fig. 1b). Due to the immiscibility between heptane and water, TPE only covered one part of the CNTs exposed to the air side, while the CNTs immersed in the water phase will be significantly preserved. The CNTs in the hybrid film tend to form interconnected networks inside the TPE matrix. When stretching the hybrid film to a certain strain, it can have a corresponding current change due to the mechanism of stretching inducing the increase of the contact resistance inside the CNT networks. After releasing the strain, the conductivity of the film can be

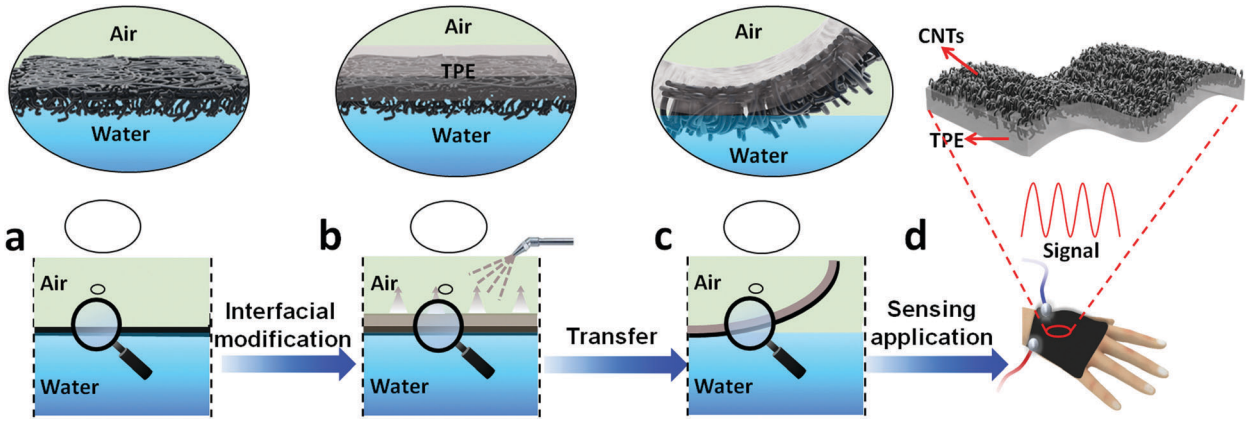

Fig. 1 The schematic illustration of the preparation of the CNT/TPE hybrid thin film. (a) A uniform CNT film was prepared using the modified Langmuir–Blodgett method at the air/water interface. (b) The CNT/TPE hybrid Janus film was formed at the air/water interface. The CNT/TPE hybrid film can be transferred to be a self-adhesive and free-standing one (c) for further sensing application (d).

restored to the original state, ensuring the potential in the mechanical sensing system. Therefore, the resultant CNT/TPE hybrid thin film can be transferred to other substrates (Fig. 1c) for further sensing applications (Fig. 1d).

Fig. 2a shows a photo image of the CNT/TPE hybrid film, which is highly uniform on a large scale. The hybrid film could be easily tailored into various geometries. Meanwhile, owing to the excellent mechanical, flexible, elastic and adjustable self-adhesion properties of TPE, the CNT/TPE hybrid film could be easily transferred onto different substrates (Fig. 2b and c) and act as a free-standing and self-adhesive flexible strain sensor. As displayed in the amplified image in Fig. 2c, the textures of the skin could be clearly observed, indicating good self-adhesivity and conformity. SEM was further used to characterize the microstructures of the hybrid film. As shown in Fig. 2d, CNTs on the air side were completely coated by TPE, showing a uniform morphology. The remarkable difference in tubular CNTs on the water side further confirmed the Janus structures (Fig. 2e).

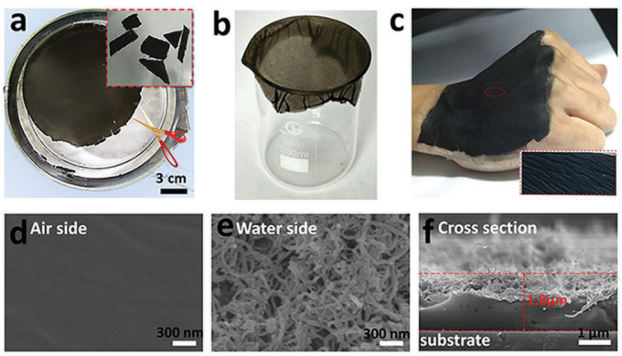

Fig. 2 (a) Photograph of the CNT/TPE hybrid film at the air/water interface. Scale bar, 3 cm. Insets: Photograph of the film that was cut into different shapes. (b) Photograph of the CNT/TPE hybrid film transferred onto a beaker. (c) Photograph of the transferred CNT/TPE hybrid film on the skin surface. Insets: Partial enlargement photograph. SEM image of the CNT/TPE hybrid film, (d) TPE layer at the air side. Scale bar, 300 nm. (e) CNT layer at the water side. Scale bar, 300 nm. (f) The cross sectional SEM image of the CNT/TPE hybrid film. Scale bar, 1 μm.

This asymmetrical structure is also evidenced from the cross-sectional image (Fig. 2f), and the thickness of the CNT/TPE hybrid film is about 2 μm. This asymmetric structure not only possesses the excellent self-adhesion of the ultrathin TPE, but maintains the good conductivity of the CNTs, which ensures successful output of the electric signal.

In order to evaluate the tension sensing performance of the CNT/TPE hybrid film, the gauge factor (GF) of the CNT/TPE hybrid film was tested. Due to its ultrathin feature, the CNT/TPE film tends to be curled, and the CNT/TPE hybrid film was coated on a flexible PDMS substrate, followed by a gradual stretching to different tensile states. The tensile strain (ε) of the CNT/TPE hybrid film can be calculated according to the equation: $\varepsilon = (L - L_0)/L_0$, where L and L_0 are the film lengths at the tensile state and the original relaxed state, respectively. The current (I) of the CNT/TPE hybrid film was measured in real time during stretching, and the resistance (R) of the CNT/TPE hybrid film can be obtained through the equation: $R = U/I$. Finally, the normalized relative resistance ($\Delta R/R_0$) was calculated using the equation: $\Delta R/R_0 = (R - R_0)/R_0$, where R_0 is the film resistance at the relaxed state, and R represents the real-time resistance.

To achieve optimized performance, the effects of different thicknesses of CNT films (Fig. S1, ESI†) and TPE (Fig. S2, ESI†) were investigated, which is shown in Fig. 3a. Considering the conductivity (Fig. S3, ESI†) and mechanical strength of the hybrid film, the appropriate film thickness (CNTs: 700 nm and TPE: 2 μm) was selected for further experiments. Significantly, there is a negative correlation between the thickness and self-adhesion. In order to provide a high-adhesive property, the hybrid film with the appropriate thickness and strength was preferable. As shown in Fig. 3b, $\Delta R/R_0$ increases monotonically with tensile strain up to ε = 50%, which demonstrated considerable sensitivity that meets the demand of applications in human motion monitoring (primary sensing target: $\varepsilon < 55\%$).[30] The GFs, as the representative parameters to access strain sensitivity, were calculated ($\Delta R/R_0/\varepsilon$) to be 0.97 (ε: 0.5–10%), 1.23 (ε: 10–30%), and 1.97 (ε: 30–50%). Fig. 3c presents the

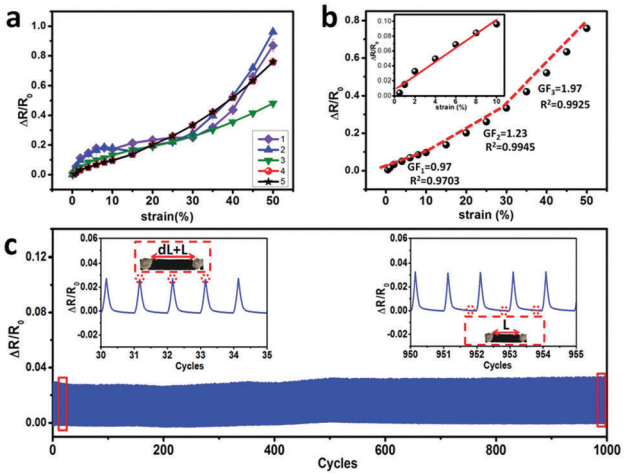

Fig. 3 (a) The normalized relative resistance *versus* strain curves of different thicknesses of CNT/TPE films. The thicknesses of the CNT films and TPE are about 250 nm and 2 μm (1), 400 nm and 2 μm (2), 500 nm and 2 μm (3), 700 nm and 2 μm (4) and 700 nm and 18 μm (5), respectively. (b) $\Delta R/R_0$ *versus* strain curve. (c) Normalized relative resistance variation under cyclic stretching from ε = 0% to ε = 1% with a frequency of 0.1 Hz over 1000 cycles, which shows the reproducibility and durability of the strain sensor.

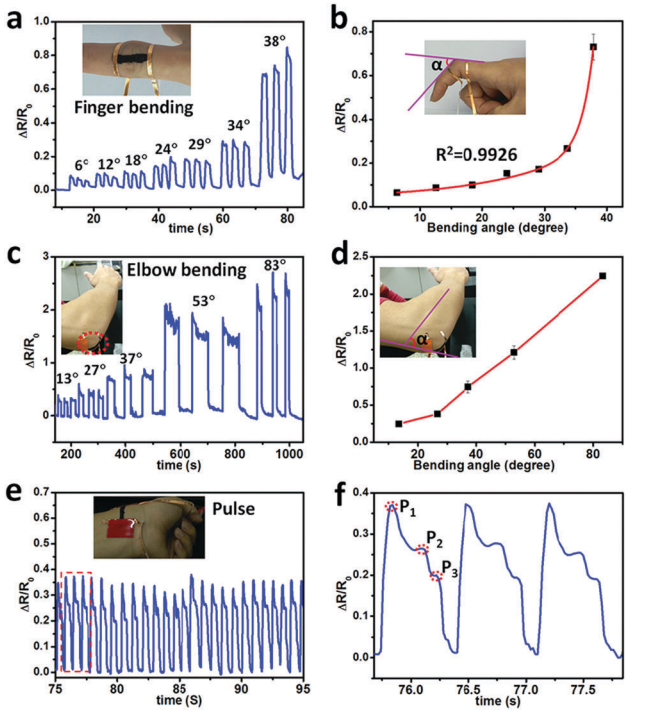

Fig. 4 Real-time human activities detection with the CNT/TPE film adhered directly to the skin surface. (a) $\Delta R/R_0$ *versus* time curve of the finger bending and releasing behaviour. Inset: Photo of CNT/TPE film attached to the knuckles. (b) $\Delta R/R_0$ *versus* bending angle curve. (c) $\Delta R/R_0$ *versus* time curve with real-time detection of the elbow joint bending. Inset: Photo of the film adhered to the elbow joint. (d) $\Delta R/R_0$ *versus* bending angle. (e) Real-time detection of the wrist pulse. Inset: Picture of film self-adhered to the wrist surface. (f) An enlarged image of the pulse detection.

resistance variation of the strain sensor during cyclic stretching from ε = 0% to ε = 1% with a frequency of 0.1 Hz over 1000 cycles. In this process, $\Delta R/R_0$ varied periodically, and the maximum value of each cycle did not show an apparent change, demonstrating the good reproducibility and durability of the sensor. After the durability tests, the morphology of the CNT/TPE hybrid film still didn't show any obvious change, demonstrating the excellent stability of the strain sensor (Fig. S4, ESI†).

Thanks to the unique self-adhesion property, the hybrid film can be directly adhered to the textured skin surface for the detection of the human motion. As displayed in Fig. 4a, the finger bending behaviour could be effectively detected, in which different bending angles (ranging from 6° to 38°) were precisely distinguished (Fig. 4b). In addition, when attached to the elbow, real-time detection of a larger deformation (up to 83°) was also achieved (Fig. 4c and d). The film was stable enough for rigorous bending and releasing cycles, demonstrating significant potential in human motion behaviour monitoring. Furthermore, even some tiny physiological signals could also be monitored. Pulse diagnosis is a traditional diagnostic method in China, providing the doctor with important physiological information on the human body. As shown in Fig. 4e, the ultrathin strain sensor can adhere tightly to the wrist surface with good skin-conformality, which can induce the formation of tiny deformations of the self-adhesive film driven by pulse vibration, resulting in a sensitive and stable wrist pulse signal (VHB tape was used to ensure good contact between the hybrid film and the copper foil). The amplified image displayed in Fig. 4f, represents a typical radial artery pulse waveform with three clearly distinguishable peaks (P1, P2 and P3). The line shape is caused by the constitution of the blood pressure from the left ventricle contracting and a reflective wave from the lower body, which provided detailed information about the stiffness and health of a person's arteries.[31–33] More importantly, the CNT/TPE sensor can represent good self-adhesivity and sensing performance even under perspiring conditions (Fig. S5, ESI†). The results strongly indicated that the hybrid film has great potential to act as a highly efficient strain sensor to monitor human physiological behaviours.

Due to the ultrathin, self-supported and self-adhesive properties, the film could be used for the detection of the weight of an object by gravitational stretching. As displayed in Fig. S3a, ESI,† this system is sensitive enough to distinguish different mass objects, ranging from rice (24.5 mg), and ormosia (222.5 mg) to cowpea (497 mg) (Fig. S6a, ESI†). The CNT/TPE hybrid film was further transferred into the bottle edge of a sealed container (such as beaker, flask and test tube) to detect the gas content changes or pressure changes. For instance, the CNT/TPE hybrid film sensor can well record the injection and extraction of air (Fig. S6b, ESI†). When covering the stopper and removing the stopper at different frequencies, the resistance of the hybrid film can experience real-time variation under the repetitive stretching induced by gas expansion (Fig. S6c, ESI†). The sensor exhibited a highly reproducible response, making it suitable for the detection of human breath (16–20 times per minute for healthy adults in a calm state) and other types of stretching with different frequencies.

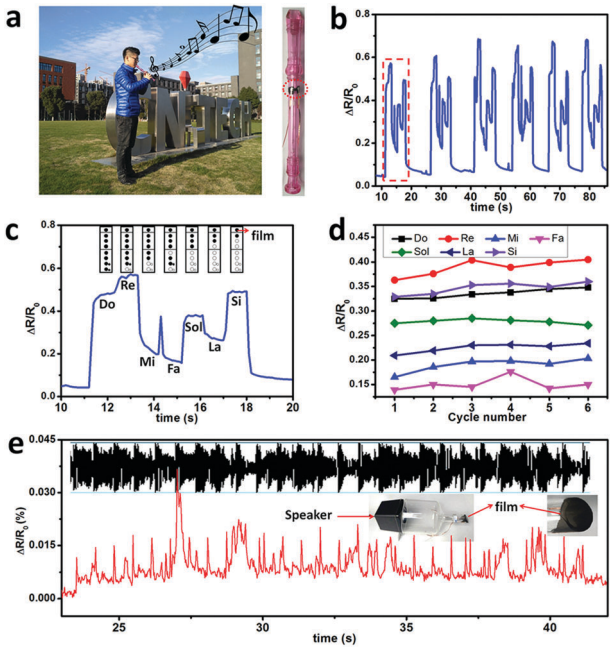

Fig. 5 Real-time detection of air flow and acoustic vibration using the CNT/TPE hybrid film strain sensor. (a) Picture of a volunteer playing the recorder. (b) Real-time $\Delta R/R_0$ *versus* time curve when blowing different musical notes. (c) The enlarged curve in (b), representing good distinguishment of every musical note. Inset: Different notes of fingering, the solid circle means holding the recorder hole, the open circle means releasing the recorder hole. (d) Statistics of $\Delta R/R_0$ curves of different musical notes. (e) Real-time monitoring of the acoustic signal by a loudspeaker. Insets: Photo of a home-made equipment to detect the eardrum.

More interestingly, the hybrid film can be employed for precise detection of even airflow in an open system. As a proof of concept, the hybrid film was attached onto the back hole of the recorder, which was used to monitor the air vibration (Fig. 5a). When blowing a different musical note (From Do, Re, Mi, Fa, Sol, La to Si) 6 times, the normalized relative resistance was acquired in Fig. 5b, demonstrating a high reproducibility (the slight difference between each cycle resulted from the slight discrepancy of each blowing rate and blowing volume). From the amplified image in Fig. 5c, we can see that every musical note could be clearly distinguished. Furthermore, the repeated experiments also evidenced the excellent recognition of every musical note (Fig. 5d). Inspired by the human eardrum, the ultrathin and self-adhesive film could be further integrated into a home-made model to mimic the structure of a real ear system. As illustrated in Fig. 5e, a loudspeaker was placed 18 cm away from the artificial electronic eardrum. Due to the excellent flexibility and sensing performance of the film, it can respond sensitively to a change in the air pressure and vibration. Once the loudspeaker played, it could effectively drive the free-standing film to stretch and release according to the rhythm, resulting in the corresponding resistance change of the film for real-time detection of the acoustic signals. The potential mechanism of acoustic signal detection is given in Fig. S7, ESI.† Both the ringtone version and full version accompaniment of the song ''diamonds'' were used for sound detection (Fig. S8, ESI†). As displayed in Fig. 5e, the sound signal can be well-detected and precisely distinguished. Meanwhile, the signal is highly repeatable. This demonstrated that the hybrid film based strain sensors have a promising prospect in sound recognition and in artificial eardrums.

Conclusions

In summary, we have described a simple and cost-effective method to fabricate an ultrathin, tailorable, transferrable, free-standing and self-adhesive CNT/TPE hybrid film at an air/water interface. The resultant film can be attached onto the textured skin surface to achieve real-time human physiological behaviour monitoring. Furthermore, based on the unique self-adhesivity and flexibility of the film, it was further employed as a free-standing film in a closed/open system, which demonstrates significant potential in detecting tiny air pressure changes and even acoustic recognition.

Conflicts of interest

There are no conflicts of interest to declare.

Acknowledgements

We thank the Natural Science Foundation of China (51573203), the Key Research Program of Frontier Science and Education of Chinese Academy of Sciences (QYZDB-SSW-SLH036), the Ningbo Science and Technology Bureau (2015C110031), and the Youth Innovation Promotion Association of Chinese Academy of Science (2016268), the Open Research Fund of Key Laboratory of Marine Materials and Related Technologies (2016Z01, 2017K03).

Notes and references

1 M. Amjadi, K.-U. Kyung, I. Park and M. Sitti, *Adv. Funct. Mater.*, 2016, **26**, 1678.
2 A. Chortos and Z. Bao, *Mater. Today*, 2014, **17**, 321.
3 M. L. Hammock, A. Chortos, B. C. Tee, J. B. Tok and Z. Bao, *Adv. Mater.*, 2013, **25**, 5997.
4 Y. Khan, A. E. Ostfeld, C. M. Lochner, A. Pierre and A. C. Arias, *Adv. Mater.*, 2016, **28**, 4373.
5 X. Wang, L. Dong, H. Zhang, R. Yu, C. Pan and Z. L. Wang, *Adv. Sci.*, 2015, **2**, 1500169.
6 N. N. Jason, M. D. Ho and W. Cheng, *J. Mater. Chem. C*, 2017, **5**, 5845.
7 D.-H. Kim, N. Lu, R. Ma, Y.-S. Kim, R.-H. Kim, S. Wang, J. Wu, S. M. Won, H. Tao, A. Islam, K. J. Yu, T. I. Kim, R. Chowdhury, M. Ying, L. Xu, M. Li, H. J. Chung, H. Keum, M. McCormick, P. Liu, Y.-W. Zhang, F. G. Omenetto, Y. Huang, T. Coleman and J. A. Rogers, *Science*, 2011, **333**, 838.
8 S. H. Jeong, S. Zhang, K. Hjort, J. Hilborn and Z. Wu, *Adv. Mater.*, 2016, **28**, 5830.
9 S. M. Lee, H. J. Byeon, J. H. Lee, D. H. Baek, K. H. Lee, J. S. Hong and S. H. Lee, *Sci. Rep.*, 2014, **4**, 6074.

10 S. Y. Yang, E. D. O'Cearbhaill, G. C. Sisk, K. M. Park, W. K. Cho, M. Villiger, B. E. Bouma, B. Pomahac and J. M. Karp, *Nat. Commun.*, 2013, **4**, 1702.
11 M. Su, F. Li, S. Chen, Z. Huang, M. Qin, W. Li, X. Zhang and Y. Song, *Adv. Mater.*, 2016, **28**, 1369.
12 M. Jian, K. Xia, Q. Wang, Z. Yin, H. Wang, C. Wang, H. Xie, M. Zhang and Y. Zhang, *Adv. Funct. Mater.*, 2017, **27**, 1606066.
13 D. J. Lipomi, M. Vosgueritchian, B. C. Tee, S. L. Hellstrom, J. A. Lee, C. H. Fox and Z. Bao, *Nat. Nanotechnol.*, 2011, **6**, 788.
14 X. Liu, C. Tang, X. Du, S. Xiong, S. Xi, Y. Liu, X. Shen, Q. Zheng, Z. Wang, Y. Wu, A. Horner and J.-K. Kim, *Mater. Horiz.*, 2017, **4**, 477.
15 X. Hu, Z. Huang, X. Zhou, P. Li, Y. Wang, Z. Huang, M. Su, W. Ren, F. Li, M. Li, Y. Chen and Y. Song, *Adv. Mater.*, 2017, **29**, 1703236.
16 Y. Park, J. Shim, S. Jeong, G. R. Yi, H. Chae, J. W. Bae, S. O. Kim and C. Pang, *Adv. Mater.*, 2017, **29**, 1606453.
17 D. M. Drotlef, M. Amjadi, M. Yunusa and M. Sitti, *Adv. Mater.*, 2017, **29**, 1701353.
18 A. Miyamoto, S. Lee, N. F. Cooray, S. Lee, M. Mori, N. Matsuhisa, H. Jin, L. Yoda, T. Yokota, A. Itoh, M. Sekino, H. Kawasaki, T. Ebihara, M. Amagai and T. Someya, *Nat. Nanotechnol.*, 2017, **12**, 907.
19 X. Li, T. Yang, Y. Yang, J. Zhu, L. Li, F. E. Alam, X. Li, K. Wang, H. Cheng, C.-T. Lin, Y. Fang and H. Zhu, *Adv. Funct. Mater.*, 2016, **26**, 1322.
20 J. J. Shao, W. Lv and Q. H. Yang, *Adv. Mater.*, 2014, **26**, 5586.
21 M. Su, Z. Huang, Y. Huang, S. Chen, X. Qian, W. Li, Y. Li, W. Pei, H. Chen, F. Li and Y. Song, *Adv. Mater.*, 2017, **29**, 1605223.
22 Z. Huang, M. Su, Q. Yang, Z. Li, S. Chen, Y. Li, X. Zhou, F. Li and Y. Song, *Nat. Commun.*, 2017, **8**, 14110.
23 L. Zhang, P. Xiao, W. Lu, J. Zhang, J. Gu, Y. Huang and T. Chen, *Adv. Mater. Interfaces*, 2016, **3**, 1600170.
24 L. Zhang, Y. Tao, P. Xiao, L. Dai, L. Song, Y. Huang, J. Zhang, S.-W. Kuo and T. Chen, *Adv. Mater. Interfaces*, 2017, **4**, 1601105.
25 D. Han, P. Xiao, J. Gu, J. Chen, Z. Cai, J. Zhang, W. Wang and T. Chen, *RSC Adv.*, 2014, **4**, 22759.
26 P. Xiao, J. Gu, C. Wan, S. Wang, J. He, J. Zhang, Y. Huang, S.-W. Kuo and T. Chen, *Chem. Mater.*, 2016, **28**, 7125.
27 J. Wang, C. McMullen, P. Yao, N. Jiao, M. Kim, J.-W. Kim, L. Liu and S. Tung, *Microfluid. Nanofluid.*, 2017, **21**, 1.
28 L. Li, Y. Bai, L. Li, S. Wang and T. Zhang, *Adv. Mater.*, 2017, **29**, 1702517.
29 P. Xiao, J. Gu, J. He, S. Wang, J. Zhang, Y. Huang, S.-W. Kuo and T. Chen, *J. Mater. Chem. C*, 2016, **4**, 9750.
30 T. Q. Trung and N. E. Lee, *Adv. Mater.*, 2016, **28**, 4338.
31 M. F. O'Rourke, J. A. Staessen, C. Vlachopoulos, D. Duprez and G. E. Plante, *Am. J. Hypertens.*, 2002, **15**, 426.
32 W. W. Nichols, *Am. J. Hypertens.*, 2005, **18**, 3S.
33 A. P. Avolio, M. Butlin and A. Walsh, *Physiol. Meas.*, 2010, **31**, R1.